THE USE OF SATELLITE DATA IN FRENCH HIGH RESOLUTION ANALYSIS

Yves Durand
Direction de la Météorologie
Paris, France

ABSTRACT

A mesoscale analysis has been developed in the French Weather Service to provide the initial conditions for a short-range weather prediction model over France (mesh size = 35 km).

The analysed variables are the same as in the prediction model and they are evaluated directly on the levels of the model and at grid points.

Since we lack conventional data in the upper layers of the atmosphere on this scale, we make use of radiances data from the NOAA's satellites (HIRS radiometer). These data have a resolution which is approximately the same as our mesh size and they are inserted directly in the analysis scheme (optimal interpolation: 3 dimensional, multivariate) without any retrieval procedures.

A first experiment was carried out in June 84. The analysis performed with satellite data was compared to the analysis performed without this information. Also the forecasts done with the model using these two analyses were compared. Our preliminary conclusion was that the impact of these satellite data in the analysis and the subsequent forecast was small but positive, particularly for the humidity related fields. In this experiment only clear radiances discriminated by means of the guess field were inserted. A new experiment has begun in April 85 with the NOAA 9 satellite. Some supplementary information related to nebulosity (from AVHRR) was also available. The corresponding tests on the analyses and forecasts with or without insertion of satellite data have been made and are reported in this paper.

1. INTRODUCTION

The "PERIDOT" project has been planned in France in order to forecast subsynoptic phenomena at short range (less than 36 hours) over France by making the best use of all small scale information, including satellite data.

It has been developed so that it has three components :

- an analysis scheme ;
- a normal mode initialization (Brière , 1982; Craplet, 1985);
- a forecast model (Pham et al, 1983).

The characteristics of the grid used by the model are an area of 51x51 points ($\simeq$ 1750 km x 1750 km) with a grid length of about 35 km, 15 sigma levels irregulary spaced and adapted orography. Pronostics variables are : Ps (surface pressure), T, $\underline{V}$ (temperature and wind) and Q (specific humidity) (Fig. 1).

2. MESOSCALE ANALYSIS

2.1. Problem definition

We have to use all the available information at this scale for operational runs. This information can be provided from three sources :

- conventional data ;
- satellite data ;
- guess-field (mesoscale forecast).

From these data we try to make maximum use of the observed parameters : the pressure in SYNOP reports, parts B and D of TEMP messages and satellite radiances at their highest resolution (a pixel definition which is compatible with our mesh size can be easily obtained and this overcomes our present incapacity to

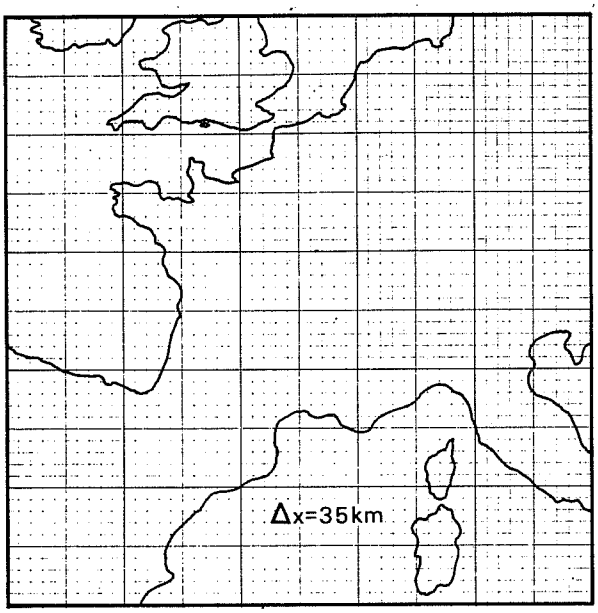

k	σ_k	r_k(mb)	Z_k(m)		$\bar{\sigma}_k$	$\bar{r}_k$(mb)	$\bar{Z}_k$(m)	k
0	0	0						
1	0,129	130	14500		0,064	65	18800	1
2	0,249	252	10300		0,189	191	12050	2
3	0,360	365	7830		0,340	308	8980	3
4	0,462	468	6050		0,411	417	6900	4
5	0,555	563	4690		0,509	516	5350	5
6	0,640	648	3610		0,598	606	4130	6
7	0,715	725	2730		0,678	687	3160	7
8	0.792	793	2020		0,749	759	2370	8
9	0,840	851	1450		0,811	822	1730	9
10	0,889	900	982		0,864	876	1210	10
11	0.929	941	618		0,909	921	789	11
12	0,960	973	343		0,944	957	480	12
13	0,982	995	151		0,971	984	247	13
14	0,995	1008	38		0,989	1002	94	14
15	1	1013,25	0		0,998	1011	19	15

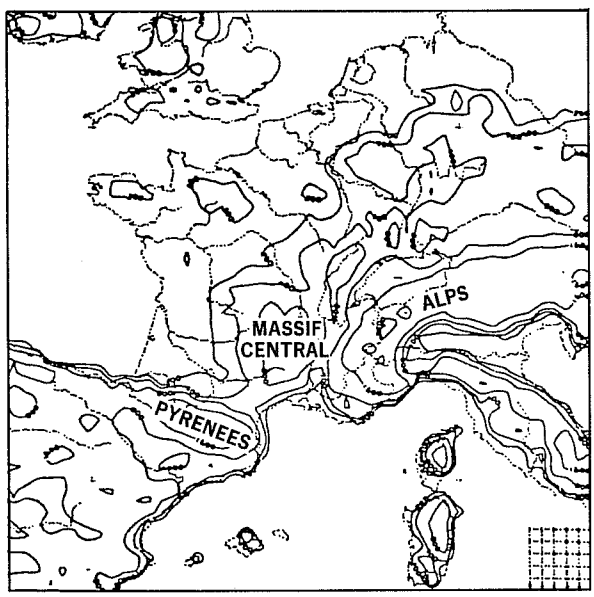

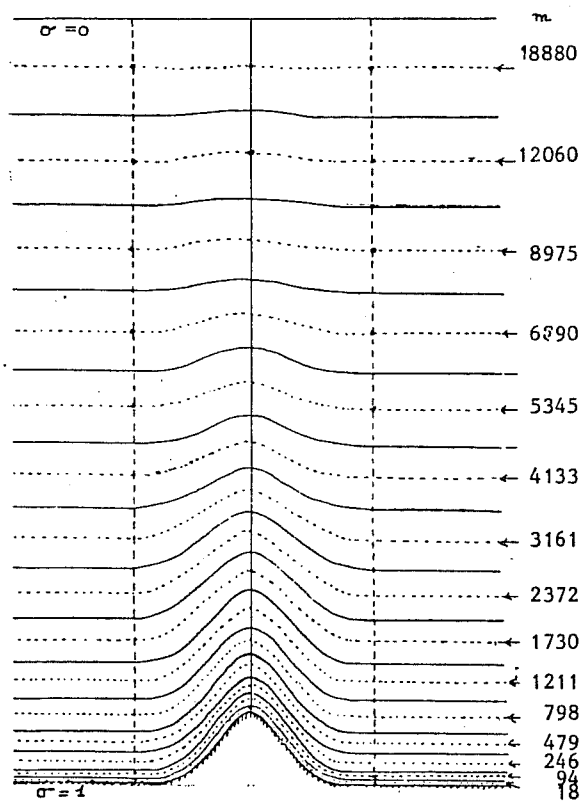

Fig. 1 Grid and levels used in the analysis.

produce operationally inversed profiles). We can also compute new parameters such as thermal winds. From the guess-field we have to make the best use of present mesoscale structures (if they exist), both horizontally and vertically, and not to modify it when there are no observations available.

One of the most important problems is to define the forcing effect of the macroscale circulation:

* The Peridot analysis does not describe the large scales (inadequate structure functions).
* The boundaries are obviously badly analysed.

2.2. Proposed solution

* Analyse all prognostic variables (except for humidity): i.e., T, $\underline{V}$, Ps on sigma levels.

* Take the maximum number of observed parameters (e.g. the observed pressure at the orographic height from SYNOP reports, 19 measured radiances in the channels of NOAA polar orbiting satellites, temperature in AIREP messages...).

* Use adapted statistical structures in the guess-field: e.g. anisotropic correlation functions for humidity, nearly univariate scheme for wind in low levels, good spectral response in a large band of waves.

* Use an optimum interpolation analysis technique in order to blend many different types of observations (radiances).

* Use a synoptic analysis on the lateral boundaries to solve problems associated with observations outside the area and blend it with the mesoscale analysis using the Davies technique.

* Keep a good macroscale component over the area (obtained from a hemispheric synoptic analysis).

2.3. Problem of the first guess

Some problems occurred because the macroscale forecast used as the guess field (after interpolation over our grid) has large scale errors (for instance temperature field too low over a large part of the area including sea) that could not be corrected sufficiently by the mesoscale analysis.

Therefore when we only analyse OZ data we use directly the hemispheric analysis (latitude - longitude grid of 1.5°x2°) interpolated on the fine-mesh grid as first guess. In practice it works well, but in reality we ignore the correlations between the guess errors and the observation errors already used in the hemispheric analysis.

Nevertheless we use as correlation functions for the guess error results obtained experimentally with the mesoscale forecast model (Fig. 6 and 9). Only the guess error variances have been tuned with the hemispheric analysis (after horizontal interpolation).

Towards the end of the year we plan to implement a discontinuous assimilation (18, 21, 00 Z) with the mesoscale forecast model providing the guess-field.

3. CONVENTIONAL OBSERVATIONS AND CORRESPONDING GUESS PARAMETERS

3.1. Synop/Ship ($\simeq$ 330 data over the area)

As indicated we use observed pressure, possibly computed with the inverse of national reductions. Temperature and wind are taken directly and we compute profiles of relative humidity with parameters such as present weather, cloud type, nebulosity (cloud amount)...

The pressure-altitude information is converted into an increment of geopotential at the observed pressure by interpolating the guess geopotential at this pressure (hypothesis : T linear in log of pressure). The guess value for wind is the available 2 metre

wind, but for temperature we take the 15 metre temperature guess (first altitude level) with a correction for the difference between the model and real orographic height.

3.2. Temp/pilot ($\simeq$ 31 data over the area)

We use the geopotential, wind and temperature at every level of parts B and D. In the middle of these layers we compute the thermal wind. The corresponding guess values are deduced by vertical interpolation from a profile of the pronostic variables (T, V, Ps). A polynomial integration is performed over the relative humidity layers with both the observed and the guess profiles.

3.3. Others observations ($\simeq$ 30 data)

* Airep/Asdar : wind and temperature are used.

* Satob : wind only is used.

4. SATELLITE INFORMATION

4.1. General use

The need to get early mesoscale satellite observations leads us to consider the use of radiances from the NOAA polar orbiting satellites directly received at Lannion (Centre de Météorologie Spatiale) in France. In the horizontal, the satellite pixel has about the same definition as our analysis grid but vertically a radiance is generally representative of a thickness larger than our analysis layers (especially in low levels), so there is vertical smoothing at these levels. Moreover only a few channels can describe low atmospheric layers where we find most of the analysis levels and these channels have proportionally high observation errors.

Nevertheless we have a network of observations at the surface which captures mesoscale features and can represent them in the analysis ; the main problem is at higher levels where the

conventional network is too sparse to get a mesoscale analysis. Therefore the introduction of some 200 satellite pixels is necessary if we want to have some information on our grid resolution and not to only reproduce the guess field with small corrections here and there.

In addition to the radiance data (HIRS radiometer, 19 channels), the Lannion Centre sends us the result of a histogram analysis of AVHRR radiometer pixels ($\simeq$ 2 Km definition) inside one HIRS pixel ($\simeq$ 30 Km definition). The different classes give an indication of the nebulosity, ground temperature, number of clouds in the pixel and the radiative temperatures. Therefore by decoding these results we can discriminate between clear pixels where we use directly observed radiances and completely covered pixels with a uniform cloud cover where we produce relative humidity bogus data. In many cases we cannot reach any conclusion (e.g. clouds at different levels or a partially covered pixel). As we do not use actual micro-wave radiometer data (a too large definition both horizontally and vertically), clouds form a barrier ; therefore in this case we plan to use only channels providing information about layers situated above the clouds.

Another problem is the calculation of synthetic radiances from a guess profile of temperature, humidity and surface parameters; we take a climatic value of ozone content. For this we use a NOAA subroutine whose internal statistical characteristics errors are unknown. But in our case the most serious limitation in its use and in its results is that we have very few levels at high altitude, so we get only an approximate result for some channels which would be of interest at levels where very few others observations are available.

Another limitation comes from the evaluation of surface variables (surface temperature, albedo) at our scale which can be very false even if we use a synoptic analysis as the guess field.

4.2. Statistics about the radiance guess errors

For the OI scheme we need information about variances and covariances involving synthetic radiance guess errors in each channel and for every satellite. Synthetic radiances are obtained from a guess profile. Therefore the guess error of every term of this profile adds to the error of the subroutine to give the final error of the synthetic radiance. We have also to know the cross-correlations between these errors and the geopotential, temperature and humidity guess error. Later we will use the following notations :

$\mathcal{E}R_i^{g\alpha}$: error of synthetic radiance due to the profile errors at vertical i in channel α

$\mathcal{E}'R_i^{\alpha}$: error of the subroutine.

We are going to apply a kind of "Monte-Carlo" method. Knowing all guess error variances and covariances between the geopotential, temperature and humidity at every level we can easily simulate a profile of these variables at every level (by using a Gaussian law for instance) corresponding to the fixed covariances. These profiles of error are used to modify a "true" profile (in fact a radiosonde profile at midlatitude). The difference in synthetic radiance obtained between the "true profile" and the "erroneous" one gives, as a first approximation, an evaluation of the synthetic guess radiance error (error due to the errors in the profile : $\mathcal{E}R_i^{g\alpha}$) but no indication about the error due to the subroutine ($\mathcal{E}'R_i^{\alpha}$).

By selecting a lot of soundings at the latitude of our model we can experimentally compute the required correlation error matrix between all quantities (geopotential, temperature, humidity, radiance). The computations were done with about 100 radiosondes on which we did 10 statistical experiments (Fig. 2).

CORR T/RAD SUR 11 NIVEAUX $r(T^g, R^g)$

1000	-0.020	-0.040	-0.050	0.060	0.250	0.280	0.600	0.700	0.650	0.490	0.190	0.040	0.760	0.490	0.200	0.010	0.000	0.800	0.800
850	0.010	0.000	-0.020	0.100	0.450	0.350	0.450	0.290	0.230	0.330	0.100	-0.020	0.570	0.700	0.350	0.150	0.010	0.360	0.310
700	0.150	0.090	0.100	0.140	0.500	0.550	0.400	0.190	0.050	0.270	0.220	0.050	0.410	0.580	0.590	0.200	0.080	0.230	0.200
500	0.050	0.020	0.200	0.180	0.750	0.440	0.150	0.070	0.020	0.100	0.120	0.090	0.220	0.400	0.740	0.250	0.080	0.120	0.080
400	0.120	0.060	0.300	0.250	0.600	0.360	0.070	0.060	0.070	0.080	0.090	0.100	0.140	0.210	0.490	0.500	0.170	0.090	0.070
300	0.220	0.110	0.400	0.430	0.450	0.150	0.030	0.060	0.070	0.050	0.010	0.040	0.050	0.140	0.260	0.650	0.220	0.070	0.060
250	0.340	0.250	0.550	0.680	0.300	0.080	0.000	0.060	0.070	0.050	0.030	0.080	0.020	0.080	0.150	0.700	0.270	0.060	0.060
200	0.400	0.450	0.690	0.590	0.200	-0.010	-0.060	-0.020	-0.020	-0.030	-0.010	0.020	-0.070	-0.040	0.040	0.570	0.330	-0.030	-0.020
150	0.490	0.620	0.800	0.500	0.100	0.060	-0.040	-0.070	-0.080	-0.060	-0.020	0.000	-0.080	-0.030	0.090	0.500	0.390	-0.080	-0.070
100	0.650	0.800	0.860	0.450	0.050	0.150	-0.010	-0.110	-0.130	-0.090	-0.020	-0.010	-0.090	-0.020	0.190	0.400	0.460	-0.120	-0.120
50	0.750	0.720	0.650	0.400	0.030	0.220	0.080	-0.010	-0.010	0.000	0.000	0.000	0.000	0.050	0.200	0.270	0.590	-0.010	-0.010

CORR Z/RAD SUR 11 NIVEAUX $r(Z^g, R^g)$

1000	-0.280	-0.220	-0.130	-0.300	-0.380	-0.270	-0.100	-0.040	-0.070	-0.010	-0.010	0.020	-0.190	-0.340	-0.470	-0.350	-0.290	-0.040	0.050
850	-0.200	-0.180	-0.140	-0.360	-0.310	-0.180	0.020	0.130	0.180	0.140	-0.020	-0.020	0.100	-0.120	-0.370	-0.400	-0.320	0.200	0.200
700	-0.170	-0.140	-0.180	-0.380	-0.200	-0.030	0.110	0.210	0.190	0.170	0.030	-0.010	0.240	0.070	-0.280	-0.390	-0.280	0.250	0.250
500	-0.160	-0.210	-0.250	-0.330	-0.020	0.130	0.260	0.160	0.170	0.150	0.080	0.060	0.390	0.310	0.050	-0.290	-0.250	0.260	0.230
400	-0.230	-0.260	-0.380	-0.370	0.030	0.300	0.170	0.150	0.150	0.140	0.060	0.040	0.290	0.320	0.130	-0.250	-0.200	0.210	0.190
300	-0.200	-0.350	-0.330	-0.140	0.120	0.310	0.130	0.080	0.100	0.080	0.030	0.010	0.210	0.330	0.320	-0.120	-0.160	0.130	0.100
250	-0.160	-0.320	-0.320	-0.080	0.150	0.250	0.060	0.020	0.070	0.020	0.010	0.020	0.130	0.350	0.330	-0.010	-0.130	0.090	0.050
200	-0.130	-0.270	-0.230	0.050	0.170	0.180	0.080	0.060	0.080	0.060	0.030	0.030	0.150	0.300	0.350	0.120	-0.100	0.110	0.080
150	-0.060	-0.220	-0.150	0.140	0.180	0.170	0.060	0.020	0.030	0.030	0.020	0.010	0.090	0.240	0.370	0.220	-0.090	0.040	0.030
100	0.050	-0.100	-0.010	0.260	0.220	0.170	0.030	-0.010	0.030	0.000	0.000	0.010	0.060	0.230	0.370	0.320	-0.080	0.040	0.020
50	0.180	0.300	0.370	0.470	0.320	0.200	0.040	-0.020	-0.020	0.000	0.020	0.030	0.030	0.200	0.380	0.550	0.080	-0.010	-0.020

CORR ERR RAD SYNTH GUESS $r(R^g, R^g)$

1	1.00	0.95	0.96	0.81	0.44	0.08	-0.02	-0.05	-0.05	-0.05	0.03	-0.03	-0.05	-0.03	0.13	0.76	0.83	-0.05	-0.05
2	0.95	1.00	0.98	0.73	0.36	0.04	-0.02	-0.04	-0.04	-0.03	0.00	-0.05	-0.04	-0.05	0.03	0.62	0.62	0.01	0.01
3	0.96	0.98	1.00	0.82	0.37	0.00	0.00	0.00	0.00	0.00	0.00	0.00	0.00	0.00	0.00	0.75	0.73	0.00	0.00
4	0.81	0.73	0.82	1.00	0.57	0.13	0.00	0.00	0.00	0.00	0.15	0.16	0.00	0.00	0.33	0.97	0.77	0.00	0.00
5	0.44	0.36	0.37	0.57	1.00	0.87	0.72	0.62	0.59	0.65	0.43	0.24	0.65	0.73	0.91	0.50	0.43	0.60	0.61
6	0.08	0.04	0.00	0.13	0.87	1.00	0.96	0.89	0.84	0.92	0.42	0.20	0.91	0.95	0.88	0.07	0.11	0.86	0.87
7	-0.02	-0.02	0.00	0.00	0.72	0.96	1.00	0.97	0.93	0.98	0.32	0.14	0.98	0.97	0.77	-0.07	0.07	0.94	0.95
8	-0.05	-0.04	0.00	0.00	0.62	0.89	0.97	1.00	0.99	0.99	0.19	0.06	0.99	0.97	0.71	-0.09	-0.04	0.95	0.95
9	-0.05	-0.04	0.00	0.00	0.59	0.84	0.93	0.99	1.00	0.98	0.16	0.05	0.98	0.95	0.69	-0.08	-0.05	0.95	0.95
10	-0.05	-0.03	0.00	0.00	0.65	0.92	0.98	0.99	0.98	1.00	0.25	0.10	0.99	0.98	0.72	-0.09	-0.03	0.95	0.95
11	0.03	0.00	0.00	0.15	0.43	0.42	0.32	0.19	0.16	0.25	1.00	0.87	0.20	0.24	0.28	0.03	0.06	0.16	0.18
12	-0.03	-0.02	0.00	0.16	0.24	0.20	0.14	0.06	0.05	0.10	0.87	1.00	0.06	0.08	0.12	0.05	-0.01	0.05	0.06
13	-0.05	-0.04	0.00	0.00	0.65	0.91	0.98	0.99	0.98	0.99	0.20	0.06	1.00	0.99	0.75	-0.09	-0.04	0.99	0.99
14	-0.03	-0.05	0.00	0.00	0.73	0.95	0.97	0.97	0.95	0.98	0.24	0.08	0.99	1.00	0.83	-0.04	0.01	0.96	0.97
15	0.13	0.03	0.00	0.33	0.91	0.88	0.77	0.71	0.69	0.72	0.28	0.12	0.75	0.83	1.00	0.32	0.25	0.70	0.71
16	0.76	0.62	0.75	0.97	0.50	0.07	-0.07	-0.09	-0.08	-0.09	0.03	0.05	-0.09	-0.04	0.32	1.00	0.82	-0.09	-0.09
17	0.83	0.62	0.73	0.77	0.43	0.11	0.07	-0.04	-0.05	-0.03	0.06	-0.01	-0.04	0.01	0.25	0.82	1.00	-0.04	-0.04
18	-0.05	0.01	0.00	0.00	0.60	0.86	0.94	0.95	0.95	0.95	0.16	0.05	0.99	0.96	0.70	-0.09	-0.04	1.00	0.95
19	-0.05	0.01	0.00	0.00	0.61	0.87	0.95	0.95	0.95	0.95	0.18	0.06	0.99	0.97	0.71	-0.09	-0.04	0.95	1.00
	1	2	3	4	5	6	7	8	9	10	11	12	13	14	15	16	17	18	19

Fig. 2 Synthetic radiance errors based on the 6 h forecasts.

This method, by ignoring the subroutine error, does not allow us to deduce the real magnitude of synthetic radiance error, nor the possible correlations of subroutine error with profile error. This factor can contribute to an underestimation of the impact of radiances.

The "horizontal" correlation between the synthetic radiance errors is assured to be the same as for temperature errors (radius of influence varying from 500 km near the surface to 750 km at higher levels).

4.3 Radiance observation error

For every run of the analysis program with NOAA 9 radiances included, we compute the mean and variance of radiance increments by substracting the variance of $\mathcal{E}R_i^{g\alpha}$:

$$\text{increment of channel } \alpha \text{ at vertical } i = R_i^{o\alpha} - R_i^{g\alpha}$$

$$\text{(observed minus synthetic radiance)} = \mathcal{E}R^{o\alpha} - \mathcal{E}R_i^{g\alpha} - \mathcal{E}'R_i^{\alpha}$$

with $\mathcal{E}R^{o\alpha}$ = radiance observation error in channel α .

If we suppose that the three terms are uncorrelated (not obvious between $\mathcal{E}R^{g}$ and $\mathcal{E}'R$) we get :

$$\text{Var}\,(R_i^{o\alpha} - R_i^{g\alpha}) = \text{Var}\,(\mathcal{E}R_i^{o\alpha} - \mathcal{E}'R_i^{\alpha}) + \text{Var}\,(\mathcal{E}R_i^{g\alpha})$$

We did not do other studies with these data because of possible correlations in the guess field ($\mathcal{E}R^{g}$) which could superpose the structure of radiance observation errors. We noted too the very important bias for channel 16 whose variance seems to have a plausible magnitude (Fig. 3).

A more complete study was recently done with an orbit of NOAA 7 in March 1982. We obtained radiance data over a large area (larger than for the analysis) and at this time the radiosonde network was a little denser than usual due to the Alpex

experiment. We compared 100 collocated observed clear radiances and radiosonde synthetic radiances (maximum horizontal separation :1°, maximum time separation : 2 hours) (Fig. 4).

We first computed the covariance matrix of these differences. By substracting the covariance matrix of radiance error due to the errors of sounding profiles (obtained as in 4.2. with the correlation matrix of sounding error) we obtained the correlation matrix of the difference : $\mathcal{E}R^{o\alpha} - \mathcal{E}'R^{\alpha}$. We must remember that this refers to the NOAA 7 satellite and the corresponding version of the synthetic radiance subroutine. This correlation matrix, though derived using another satellite, was still used for NOAA 9 with the variances deduced previously (Fig. 5).

At this stage we decided to ignore all previous studies that we had done with less observations and we tried to do a horizontal separation of these differences between observed radiance errors and radiosondes synthetic radiance errors. The purpose is to find a simple model of the likely horizontal structure of radiance observation error. We could not define a horizontal correlation of observation error for channels 7 to 14 (except perhaps for channels 11 and 12) and for channels 18 and 19 ; all these channels correspond to surface or low level temperature. The structure functions of these channels seem very random and keep the same mean value over short distances. The other channels do not present the same characteristics and in spite of large noise at large distances due to the low number of couples and possible errors due to the clouds, they had a horizontal structure. It is very likely that a part of this structure represents variations of mean values at large distance but we can imagine the existence of a horizontal correlation in some channels for the variable $\mathcal{E}R_i^{o\alpha} - \mathcal{E}'R^{\alpha}$. In practice we model the correlation function for these channels by a polynomial with a radius of influence varying with the channel.We take into account the horizontal correlation between two channels by multiplying the covariance term between the errors in the two channels at the same profile by the mean of the horizontal correlations for each channel.

LEVEL	CHANNEL	STD GUESS ERROR $\sigma\varepsilon R^g$	STD INCREMENT $\sigma(\varepsilon R^o-\varepsilon' R-\varepsilon R^g)$	BIAS INCREMENT $\overline{\varepsilon R^o-\varepsilon' R-\varepsilon R^g}$	STD OBS ERROR $\sigma(\varepsilon R^o-\varepsilon' R)$
30	1	2.2	3.3	0.4	2.4
60	2	1.2	1.5+	-0.2	.9 *
100	3	1.15	1.4	-1.1	.8
250	4	1.1	1.5	-2.5	1.1 *
500	5	1.1	2.7	-1.7	2.45
750	6	1.15	3.0	-3.2	2.7
900	7	1.3	3.2	-2.9	3.0
SFC	8	1.15	4.	-4.9	3.7
25	9	1.1	3.6	-30.9	3.3
900	10	1.4	3.5	-4.1	3.1
600	11	2.3	3.	-3.7	2.0
400	12	3.15	4.1	-2.7	2.7
950	13	1.1	3.2	-6.3	3.0
850	14	1.1	3.	-2.9	2.8
700	15	1.1	2.9	-2.2	2.6
600	16	1.15	3.2+	27.1+	2.7 *
5	17	1.2	1.7+	-1.8	1.2 *
SFC	18	1.15	3.5+	-2.7	3.3 *
SFC	19	1.15	3.4	-2.7	3.2

* : ≠ NOAA7
\+ : Probable cause

Fig. 3 Radiance observation errors (NOAA 9 HIRS channels) based on comparisons with the guess field.

LEVEL	CHANNEL	STD RS ERROR $\sigma\varepsilon R^{rs}$	STD DIFF $\sigma(\varepsilon R^{o}-\varepsilon R'-\varepsilon R^{rs})$	RADIUS OF INFLUENCE OF HOR CORR	STD OBS ERROR $\sigma(\varepsilon R^{o}-\varepsilon' R)$
30	1	.8	2.7	1000	2.6
60	2	.7	2.2	800	2.0 *
100	3	.7	1.2	800	1.0
250	4	.5+	1.6	500	1.6 *
500	5	.5	2.6	1000	2.5
750	6	.5	2.8	500	2.7
900	7	.6	3.	0	3.0
SFC	8	.6	3.3	0	3.2
25	9	.5	2.9	0	2.8
900	10	.7	2.8	0	2.8
600	11	1.4	2.6	0	2.2
400	12	1.7	3.6	0	3.1
950	13	.5	2.8	0	2.7
850	14	.5	3.	0	2.9
700	15	.5	2.6	500	2.5
600	16	.5	1.7	1000	1.6 *
5	17	.9	2.2	800	2.0 *
SFC	18	.5	2.5	0	2.5 *
SFC	19	.5	2.8	0	2.7

* : ≠ NOAA9
\+ : Probable cause

Fig. 4 Radiance observation errors (NOAA 7 HIRS channels) based on comparisons with soundings.

MAT DE CORR D ERREUR D OBS DE RADIANCE

1	1.00	.72	.73	-.51	-.51	-.51	-.50	-.47	-.08	-.42	-.55	-.59	-.35	-.38	-.27	.69	.74	-.08	.27
2	.72	1.00	.74	-.54	-.52	-.52	-.50	-.45	-.14	-.43	-.57	-.60	-.35	-.39	-.35	.62	.69	-.05	.26
3	.73	.74	1.00	-.49	-.44	-.44	-.41	-.35	.02	-.32	-.53	-.58	-.24	-.28	-.23	.65	.70	.01	.25
4	-.51	-.54	-.49	1.00	.75	.74	.73	.71	.66	.71	.73	.64	.70	.71	.70	-.39	-.49	.52	-.01
5	-.51	-.52	-.44	.75	1.00	.75	.74	.73	.67	.73	.73	.62	.72	.73	.70	-.40	-.49	.55	.03
6	-.51	-.52	-.44	.74	.75	1.00	.75	.73	.67	.73	.73	.62	.72	.73	.69	-.42	-.50	.56	.04
7	-.50	-.50	-.41	.73	.74	.75	1.00	.75	.68	.74	.72	.59	.73	.73	.67	-.44	-.50	.58	.07
8	-.47	-.45	-.35	.71	.73	.73	.75	1.00	.68	.75	.70	.56	.74	.72	.65	-.44	-.47	.61	.11
9	-.08	-.14	.02	.66	.67	.67	.68	.68	1.00	.70	.62	.43	.71	.70	.67	-.04	-.06	.62	.31
10	-.42	-.43	-.32	.71	.73	.73	.74	.75	.70	1.00	.71	.57	.75	.73	.68	-.34	-.40	.61	.13
11	-.55	-.57	-.53	.73	.73	.73	.72	.70	.62	.71	1.00	.69	.69	.70	.68	-.43	-.53	.53	.02
12	-.59	-.60	-.58	.64	.62	.62	.59	.56	.43	.57	.69	1.00	.55	.58	.60	-.44	-.58	.33	-.07
13	-.35	-.35	-.24	.70	.72	.72	.73	.74	.71	.75	.69	.55	1.00	.74	.69	-.28	-.34	.24	.22
14	-.38	-.39	-.28	.71	.73	.73	.73	.72	.70	.73	.70	.58	.74	1.00	.73	-.27	-.36	.62	.18
15	-.27	-.35	-.23	.70	.70	.69	.67	.65	.67	.68	.68	.60	.69	.73	1.00	-.07	-.22	.57	.19
16	.69	.62	.65	-.39	-.40	-.42	-.44	-.44	-.04	-.34	-.43	-.44	-.28	-.27	-.07	1.00	.72	-.08	.26
17	.74	.69	.70	-.49	-.49	-.50	-.50	-.47	-.06	-.40	-.53	-.58	-.34	-.36	-.22	.72	1.00	-.07	.30
18	-.08	-.05	.01	.52	.55	.56	.58	.61	.62	.61	.53	.33	.24	.62	.57	-.08	-.07	1.00	.62
19	.27	.26	.25	-.01	.03	.04	.07	.11	.31	.13	.02	-.07	.22	.18	.19	.26	.30	.62	1.00
	1	2	3	4	5	6	7	8	9	10	11	12	13	14	15	16	17	18	19

Fig. 5 Observation error correlation between channels.

$$n\left[(\varepsilon R^{o}-\varepsilon' R)^{i}(\varepsilon R^{o}-\varepsilon' R)^{j}\right]$$

$$\overline{(\varepsilon R_i^{o\alpha} - \varepsilon' R_i^{\alpha})(\varepsilon R_j^{o\beta} - \varepsilon' R_j^{\beta})} =$$

$$= \overline{(\varepsilon R_i^{o\alpha} - \varepsilon' R_i^{\alpha})(\varepsilon R_i^{o\beta} - \varepsilon' R_i^{\alpha})} \times \frac{1}{2}(r_{ij}^{o\alpha} + r_{ij}^{o\beta})$$

$\left.\begin{matrix}\alpha\\ \beta\end{matrix}\right\}$ channel $\qquad\qquad$ $\left.\begin{matrix}i\\ j\end{matrix}\right\}$ profile

$r_{ij}^{o\alpha}$: horizontal correlation of observation error between profiles i and j in channel α with $r_{ii}^{o\alpha} = 1 \quad \forall \alpha, i$.

Therefore we did not try to separate the two sources of error. According to their real (and badly known) statistical characteristics, our model is more or less realistic; for instance we have a "white noise" term (having variance but no correlation in space or between channels). The correlation between the same channel at two different locations is doubtless overestimated, but not the correlation between two different channels.

We see that the term $\varepsilon' R^{\alpha}$, not taken into account with the guess error is inducted into the observation error term. It never appears on the right hand side of the linear system of analysis equation; it can only serve to decrease the weight of radiance observations.

In order for the linear system equations of the OI scheme to have a good stability (presence of channels which are highly correlated) we assume in practise that only 90% of the standard deviation of the term ($\varepsilon R^{o\alpha} - \varepsilon' R$) is correlated in space and between channels.

5. OI STATISTICAL MODEL

5.1. Temperature and wind analyses

The classical basic hypothesis is the statistical modelling of the covariance of geopotential error ; after that statistical assumptions are made about random variables that we use. That implies that horizontal and vertical correlations can be modelled as follows :

$$\overline{\varepsilon z_i^g \varepsilon z_j^g} = \sigma\varepsilon z_i^g \times \sigma\varepsilon z_j^g \times r_{zz}^{hg}(d_{ij}) \times r_{zz}^{vg}(\ln p_i, \ln p_j)$$

$\sigma\varepsilon z_i^g$ is the standard deviation of guess geopotential error.

r_{zz}^{hg} is the horizontal correlation of geopotential depending only of the horizontal distance d_{ij}.

r_{zz}^{vg} is the vertical correlation of geopotential depending only on a vertical distance.

For historical reasons (scalar computer) the horizontal model is a polynomial (Fig. 6):

$$r_{zz}^{hg}(\varepsilon z_i^g, \varepsilon z_j^g) = r_{zz}^{hg}(d_{ij}) =$$

$$1 - 7r^2 + 8{,}75\,r^3 - 3.5\,r^5 + 0.75\,r^7$$

with $r = d_{ij}/a$ for $r < 1$.

The radius of influence "a" varies with the level from 500 km (near surface) to 800 km. We have to note that this short radius of influence is inconvenient for the modelling of wind error variances. It gives high values to these variances, so the OI scheme has the tendancy to correct with exageration the wind guess. We have to increase empirically the wind observation error to reduce this problem.

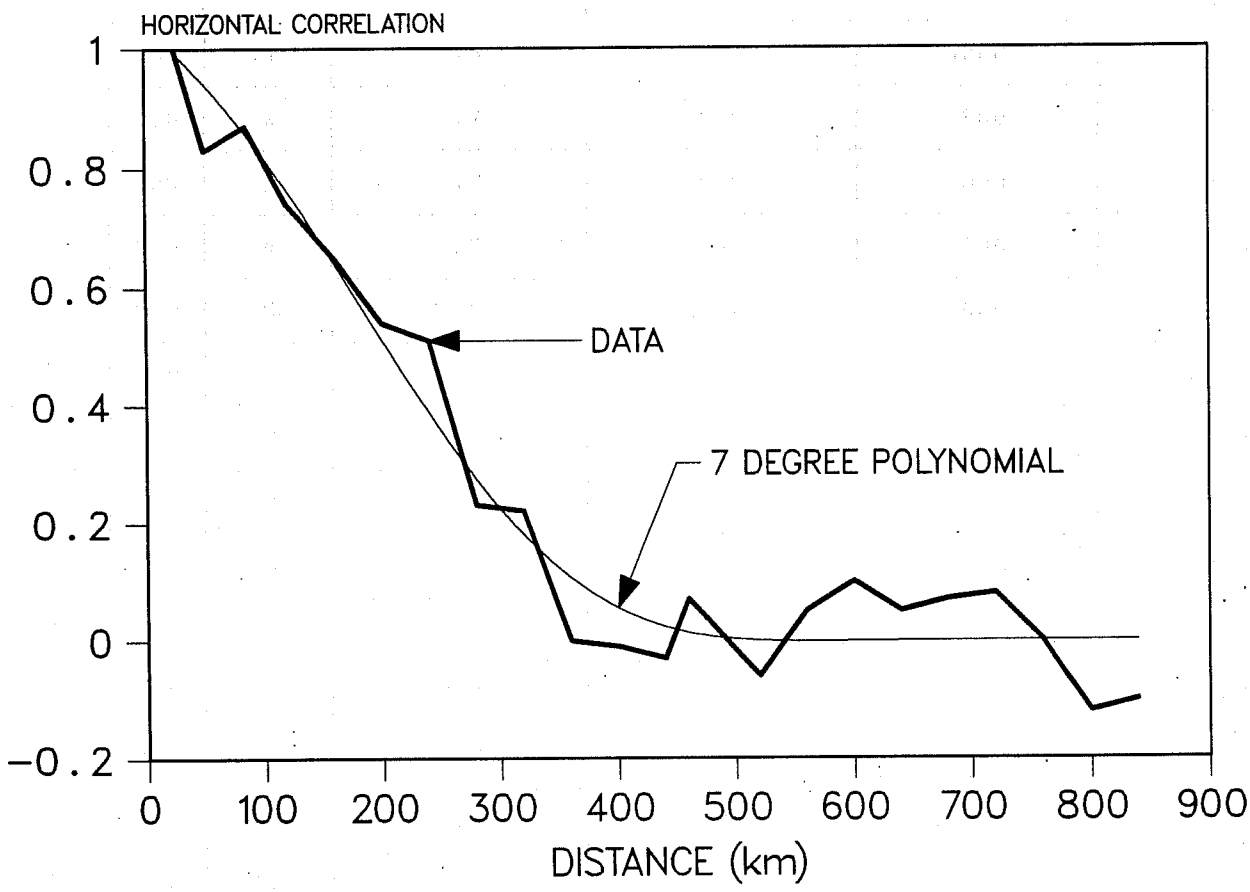

Fig. 6 Horizontal correlation of 12 h forecast errors of mean sea level pressure.
Thick line = evaluation of the horizontal correlation using real data (00 GMT, 21/9/80).
Thin line = approximation to the correlation using a 7 degree polynomial.

However some recent studies have shown that Bessel functions are particularly appropriate for small scales, so we plan to use them.

Vertically we use the same function as Bergman (1979) with the coefficient "k" varying with the level. This coefficient also determines the temperature error variance :

$$r^{vg}_{zz}(\varepsilon z^g_i, \varepsilon z^g_j) = r^{vg}_{zz}(\ln(z_i), \ln(z_j))$$

$$= \frac{1}{1 + k\left(\frac{\ln z_i}{\ln z_j}\right)^2}$$

The wind error is derived only from the stream function error, and the correlation between geopotential and stream function varies both with latitude and altitude in order to introduce a weaker geostrophic constraint. In very low levels an arbitrary coefficient is used to decrease the correlation between different wind components.

Temperature and thermal wind errors are obtained by the vertical derivative of geopotential and wind (hydrostatic hypothesis for the errors).

For radiances there is not a linear relation with other variables, and so we make the following hypothesis of separability :

$$r(\varepsilon R^{g\alpha}_i, \varepsilon z^g_k) = r(\varepsilon R^{g\alpha}_i, \varepsilon z^g_j) \times r^{hg}_{zz}(\varepsilon z^g_j, \varepsilon z^g_k)$$

tabulated polynomial

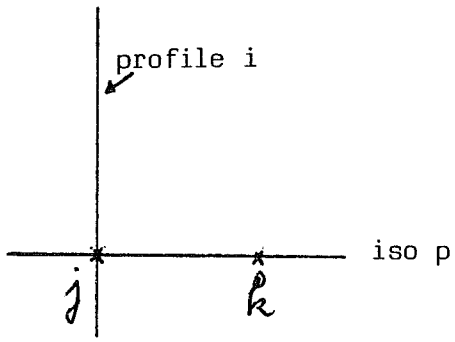

From the derivatives of this expression (written in terms of covariances) we obtain correlations with other variables : temperature, wind, thermal wind:

$$r(\varepsilon R_i^{g\alpha}, \varepsilon T_k^g) = r(\varepsilon R_i^{g\alpha}, \varepsilon T_j^g) \times r_{TT}^{hg}(\varepsilon T_j^g, \varepsilon T_k^g)$$

$$r(\varepsilon R_i^{g\alpha}, \varepsilon U_k^g) = r(\varepsilon R_i^{g\alpha}, \varepsilon Z_j^g) \times r_{ZU}^{hg}(\varepsilon Z_j^g, \varepsilon U_k^g)$$

$$r(\varepsilon R_i^{g\alpha}, \varepsilon DV_k^g) = r(\varepsilon R_i^{g\alpha}, \varepsilon T_j^g) \times r_{ZU}^{hg}(\varepsilon Z_j^g, \varepsilon U_k^g)$$

For radiance errors we take the same correlation function as for the temperature error (identical to that for geopotential) :

$$\overline{\varepsilon R_i^{g\alpha}\, \varepsilon R_j^{g\beta}} = \underbrace{\overline{\varepsilon R_i^{g\alpha}\, \varepsilon R_j^{g\beta}}}_{\text{tabulated}} \times r_{TT}^{hg}(\varepsilon T_i^g, \varepsilon T_j^g)$$

We described earlier how terms $\overline{\varepsilon R\, \varepsilon R}$, $\overline{\varepsilon R\, \varepsilon Z}$, $\overline{\varepsilon R\ \varepsilon T}$ have been tabulated.

The analysis of surface pressure is first executed with the maximum number of observations being set at 13 for every analysed point (wind and geopotential data are only used). We then modify the vertical location of altitude points (situated on sigma levels). The analysis of temperature and wind is performed simultaneously at the same points with the same set of observations. We choose the 6 best predictors for T, the 4 best predictors for the U component (not already taken) and the 3 best predictors for V. This is done in order to have consistency in analysis corrections (Fig. 7).

5.2 Humidity analysis

We took an anisotropic correlation function for the relative humidity guess error in order to retain structures contained in the guess field.

Fig. 7 General form of the OI matrix of temperature and wind. All covariances are three dimensional; the mathematical expression for each matrix block is given.
α - corr(εz_i, $\varepsilon \psi_i$)
β - factor giving the arbitary reduction of the correlation in low levels.

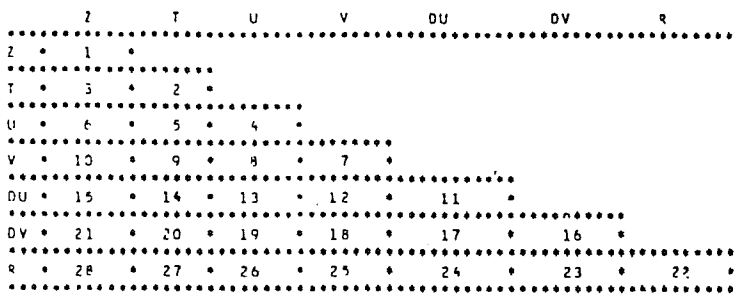

① $\overline{\varepsilon z_1^0 \varepsilon z_3^0} = \sqrt{\overline{\varepsilon z_1^{0^2}}\ \overline{\varepsilon z_3^{0^2}}}\ c^R z_1 z_2\ c^V z_2 z_3$

② $\overline{\varepsilon T_1^0 \varepsilon T_3^0} = \sqrt{\overline{\varepsilon T_1^{0^2}}\ \overline{\varepsilon T_3^{0^2}}}\ c^R z_1 z_2\ c^V T_2 T_3$

③ $\overline{\varepsilon T_1^0 \varepsilon z_3^0} = \sqrt{\overline{\varepsilon T_1^{0^2}}\ \overline{\varepsilon z_1^{0^2}}}\ c^R z_1 z_2\ c^V T_2 z_3$

④ $\overline{\varepsilon U_1^0 \varepsilon U_3^0} = \sqrt{\overline{\varepsilon U_1^{0^2}}\ \overline{\varepsilon U_3^{0^2}}}\ c^R U_1 U_2\ c^V z_2 z_3$

⑤ $\overline{\varepsilon U_1^0 \varepsilon T_3^0} = \sqrt{\overline{\varepsilon U_1^2}\ \overline{\varepsilon T_3^2}}\ c^R U_1 z_2\ c^V z_2 T_3\ \alpha$

⑥ $\overline{\varepsilon U_1^0 \varepsilon z_3^0} = \sqrt{\overline{\varepsilon U_1^2}\ \overline{\varepsilon z_3^2}}\ c^R U_1 z_2\ c^V z_2 z_3\ \alpha$

⑦ $\overline{\varepsilon V_1^0 \varepsilon V_3^0} = \sqrt{\overline{\varepsilon V_1^{0^2}}\ \overline{\varepsilon V_3^{0^2}}}\ c^R V_1 V_2\ c^V z_2 z_3$

⑧ $\overline{\varepsilon V_1^0 \varepsilon U_3^0} = \sqrt{\overline{\varepsilon V_1^{0^2}}\ \overline{\varepsilon U_3^{0^2}}}\ c^R V_1 U_2\ c^V z_2 z_3\ \beta$

⑨ $\overline{\varepsilon V_1^0 \varepsilon T_3^0} = \sqrt{\overline{\varepsilon V_1^{0^2}}\ \overline{\varepsilon T_3^{0^2}}}\ c^R V_1 z_2\ c^V z_2 T_3\ \alpha$

⑩ $\overline{\varepsilon V_1^0 \varepsilon z_3^0} = \sqrt{\overline{\varepsilon V_1^{0^2}}\ \overline{\varepsilon z_3^{0^2}}}\ c^R V_1 z_2\ c^V z_2 z_3\ \alpha$

⑪ $\overline{\varepsilon DU_1 \varepsilon DU_3} = \sqrt{\overline{\varepsilon DU_1^2}\ \overline{\varepsilon DU_3^2}}\ c^R U_1 U_2\ c^V T_2 T_3$

⑫ $\overline{\varepsilon DU_1 \varepsilon V_3} = \sqrt{\overline{\varepsilon DU_1^2}\ \overline{\varepsilon V_3^2}}\ c^R U_1 V_2\ c^V T_2 z_3\ \beta$

⑬ $\overline{\varepsilon DU_1 \varepsilon U_3} = \sqrt{\overline{\varepsilon DU_1^2}\ \overline{\varepsilon U_3^2}}\ c^R U_1 U_2\ c^V T_2 z_3$

⑭ $\overline{\varepsilon DU_1 \varepsilon T_3} = \sqrt{\overline{\varepsilon DU_1^2}\ \overline{\varepsilon T_3^2}}\ c^R U_1 z_2\ c^V T_2 T_3\ \alpha$

⑮ $\overline{\varepsilon DU_1 \varepsilon z_3} = \sqrt{\overline{\varepsilon DU_1^2}\ \overline{\varepsilon z_3^2}}\ c^R U_1 z_2\ c^V T_2 z_3\ \alpha$

⑯ $\overline{\varepsilon DV_1 \varepsilon DV_3} = \sqrt{\overline{\varepsilon DV_1^2}\ \overline{\varepsilon DV_3^2}}\ c^R V_1 V_2\ c^V T_2 T_3$

⑰ $\overline{\varepsilon DV_1 \varepsilon DU_3} = \sqrt{\overline{\varepsilon DV_1^2}\ \overline{\varepsilon DU_3^2}}\ c^R V_1 U_2\ c^V T_2 T_3\ \beta$

⑱ $\overline{\varepsilon DV_1 \varepsilon V_3} = \sqrt{\overline{\varepsilon DV_1^2}\ \overline{\varepsilon V_3^2}}\ c^R V_1 V_2\ c^V T_2 z_3$

⑲ $\overline{\varepsilon DV_1 \varepsilon U_3} = \sqrt{\overline{\varepsilon DV_1^2}\ \overline{\varepsilon U_3^2}}\ c^R V_1 U_2\ c^V T_2 z_3\ \beta$

⑳ $\overline{\varepsilon DV_1 \varepsilon T_3} = \sqrt{\overline{\varepsilon DV_1^2}\ \overline{\varepsilon T_3^2}}\ c^R V_1 z_2\ c^V T_2 T_3\ \alpha$

㉑ $\overline{\varepsilon DV_1 \varepsilon z_3} = \sqrt{\overline{\varepsilon DV_1^2}\ \overline{\varepsilon z_3^2}}\ c^R V_1 z_2\ c^V T_2 z_3\ \alpha$

㉒ $\overline{\varepsilon R_1 \varepsilon R_2} = \sqrt{\overline{\varepsilon R_1^2}\ \overline{\varepsilon R_2^2}}\ c^R T_1 T_2\ (= c^R z_1 z_2)$

㉓ $\overline{\varepsilon R_1 \varepsilon DV_3} = \sqrt{\overline{\varepsilon R_1^2}\ \overline{\varepsilon DV_3^2}}\ \cos(\varepsilon R_1 \varepsilon T_2)\ c^R z_2 V_3\ \alpha$

㉔ $\overline{\varepsilon R_1 \varepsilon DU_3} = \sqrt{\overline{\varepsilon R_1^2}\ \overline{\varepsilon DU_3^2}}\ \cdot\ \cdot\ c^R z_2 U_3\ \alpha$

㉕ $\overline{\varepsilon R_1 \varepsilon V_3} = \sqrt{\overline{\varepsilon R_1^2}\ \overline{\varepsilon V_3^2}}\ \cos(\varepsilon R_1 \varepsilon z_2)\ c^R z_2 V_3\ \alpha$

㉖ $\overline{\varepsilon R_1 \varepsilon U_3} = \sqrt{\overline{\varepsilon R_1^2}\ \overline{\varepsilon U_3^2}}\ \cdot\ \cdot\ c^R z_2 U_3\ \alpha$

㉗ $\overline{\varepsilon R_1 \varepsilon T_3} = \sqrt{\overline{\varepsilon R_1^2}\ \overline{\varepsilon T_3^2}}\ \cos(\varepsilon R_1 \varepsilon T_2)\ c^R z_2 T_3$

㉘ $\overline{\varepsilon R_1 \varepsilon z_3} = \sqrt{\overline{\varepsilon R_1^2}\ \overline{\varepsilon z_3^2}}\ \cos(\varepsilon R_1 \varepsilon z_2)\ c^R z_2 z_3$

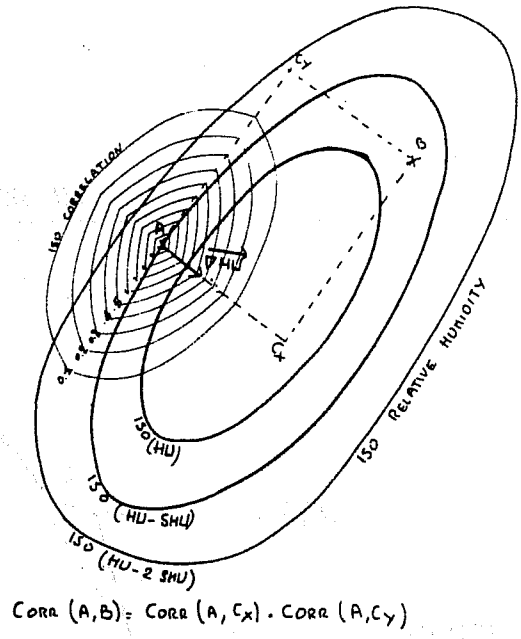

Fig. 8 Anisotropic correlation of relative humidity.

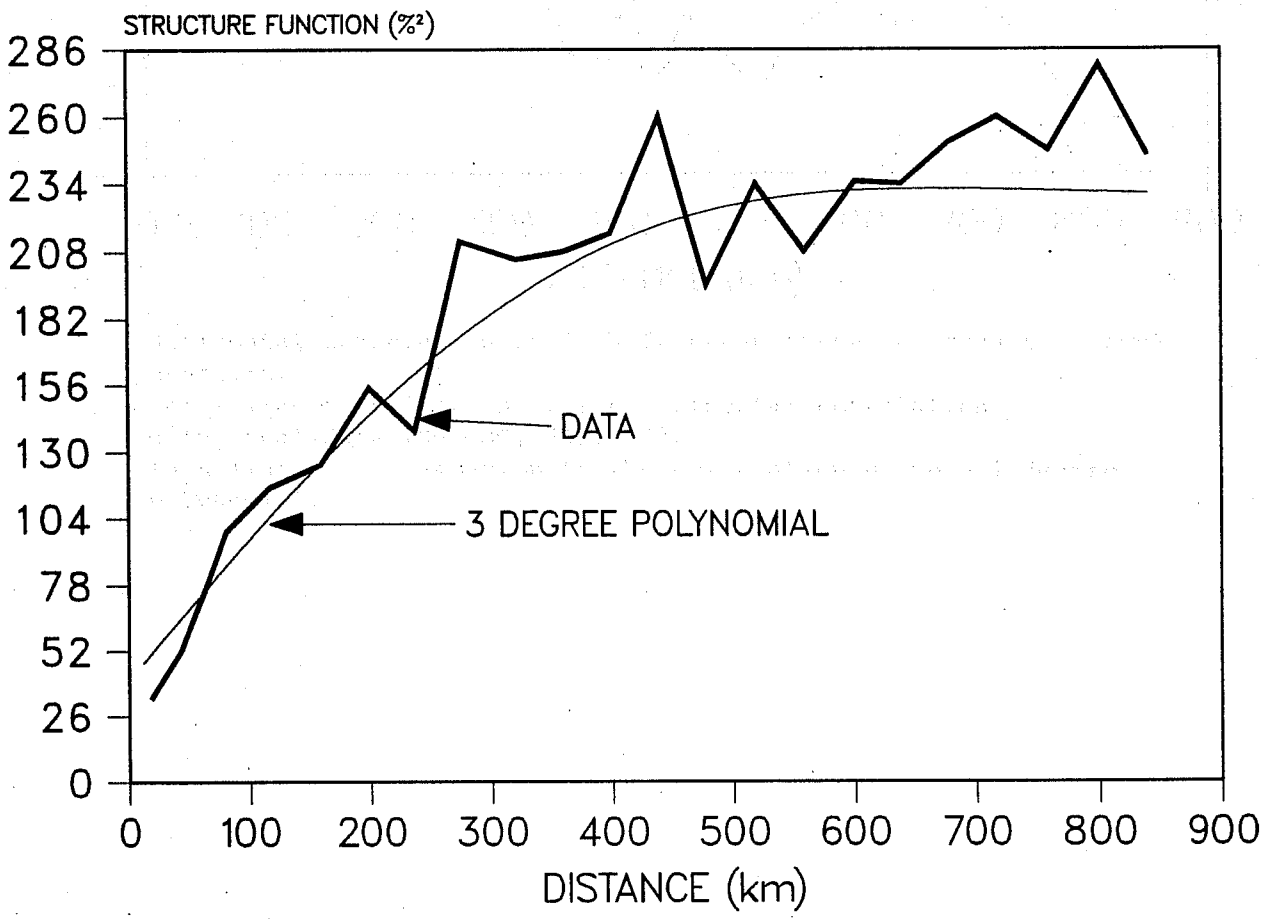

Fig. 9 Gandin structure function for the 12 h forecast error of relative humidity (units $\%^2$).
Thick line = evaluation using real data
Thin line = approximation using a 3 degree polynomial

$$r^{hg}_{HH}(\varepsilon H^g_i, \varepsilon H^g_j) = r^{hg}_{H_1}(\vec{d_{ij}}) \times r^{hg}_{H_2}(\vec{d_{ij}})$$

The two functions $r^{hg}_{H_1}$ and $r^{hg}_{H_2}$ are polynomials with a different radius of influence. The weakest correlation (small radius) is computed with the distance projected onto the guess gradient axis, whilst the other one is the projection onto the perpendicular axis (Fig. 8). The two functions are of the form :

$$r^{hg}_{H_1}(\vec{d_{ij}}) = 1 - 1.5(d_1/a_1) + 0.5(d_1/a_1)^3$$

$$r^{hg}_{H_2}(\vec{d_{ij}}) = 1 - 1.5(d_2/a_2) + 0.5(d_2/a_2)^3$$

if we decompose the vector $\vec{d_{ij}}$ into two components in a gradient depending axis system (Fig. 9).

The scheme is generally bi-dimensional but for "bogus" data a tabulated vertical correlation is used. Radiances are again inserted with a separability hypothesis :

$$r(\varepsilon R^{g\alpha}_i, \varepsilon H^g_k) =$$

$$r(\varepsilon R^{g\alpha}_i, \varepsilon H^g_j) \times r^{hg}_{HH}(\varepsilon H^g_j, \varepsilon H^g_k)$$

tabulated product of two correlations

We are not sure about the bias of the guess error of relative humidity and surface pressure, so we ensure a "universality" condition which in the general case fixes as 1 the sum of weights

corresponding to humidity observations and geopotential observations. As the radius of influence is small this condition is assured only in a small area.

5.3. Data checking

It is an important problem even at this scale to filter noise due to slightly erroneous data. By taking a hemispheric analysis as first guess we are quite sure of the veracity of the macroscale part and of the absence of large area errors.

For every observed parameter a diagnostic of doubt is produced if the parameter is too far from the guess value and different from the mean value obtained with its neighbours.

The analysis of SYNOP/SHIP data is then performed with observations which are not doubtful. It is quite impossible to also use this technique higher up where the density of observation is low, because the correlations between data are very weak due to the limited radius of influence of the horizontal correlations.

6. IMPACT OF RADIANCES

An experiment began in April 85 and is still running to examine the impact of radiances. An analysis is performed everyday at 0 Z with radiances if the time of the NOAA 9 orbit is not too late (2h30 maximum delay). A comparison is done with another analysis performed without radiances: we examine the principal analysed fields on sigma levels or interpolated on pressure levels. The results add to those from the previous experiment carried out in June 84 (J. Pailleux, 1984 ; Y. Durand and R. Juvanon du Vachat, 1985). Actually only situations from April 85 have been studied and are reported in this study.

6.1. Impact in the analysis

a) Temperature and wind : In the analysis the magnitude of the differences between the two runs is generally very small at low levels. There are differences in the details but it is very difficult to make any definite conclusion because the analyses (and the guess fields) are not very different from analyses performed with only conventional data and we lack the techniques to appreciate the mesoscale features provided by radiances data and to separate them from noise. At higher levels the differences have larger structures with greater amplitude (some degrees in temperature, a few m/s in wind) but we have the same problem of evaluation. Some analyses done without conventional data (radiances only) show that the correction implied by radiance data is compatible with these missing conventional data (same sign, but less magnitude).

b) Humidity : The impact is clearer for this parameter. The mixing of satellite "bogus" data and radiances gives high amplitude corrections which have been judged very positive (Fig. 10). Where we see a difference it is easier to compare areas with high value of humidity with satellite pictures than those with low value where we use plenty of radiances (clear air). One can ask if the impact in high values is only due to the "bogus" data; however in June 84 we had the same phenomena (increase of some high value areas), but of smaller amplitude by taking into account only clear radiances, without using any "bogus" data.

6.2. Impact in forecasts (Fig. 11)

With the set of two analyses ("WITH" and "WITHOUT" radiance) we performed two 12 hours forecasts with the mesoscale numerical model, integrated with fixed boundary conditions (hemispheric analysis, same conditions in the two runs). We shall call the experiments "WITH" and "WITHOUT".

The first result, different from those for June 84, is that the use or not of the normal mode initialization does not alter results of the experiment, whereas in June the impact of radiances could only be seen when we did not use the

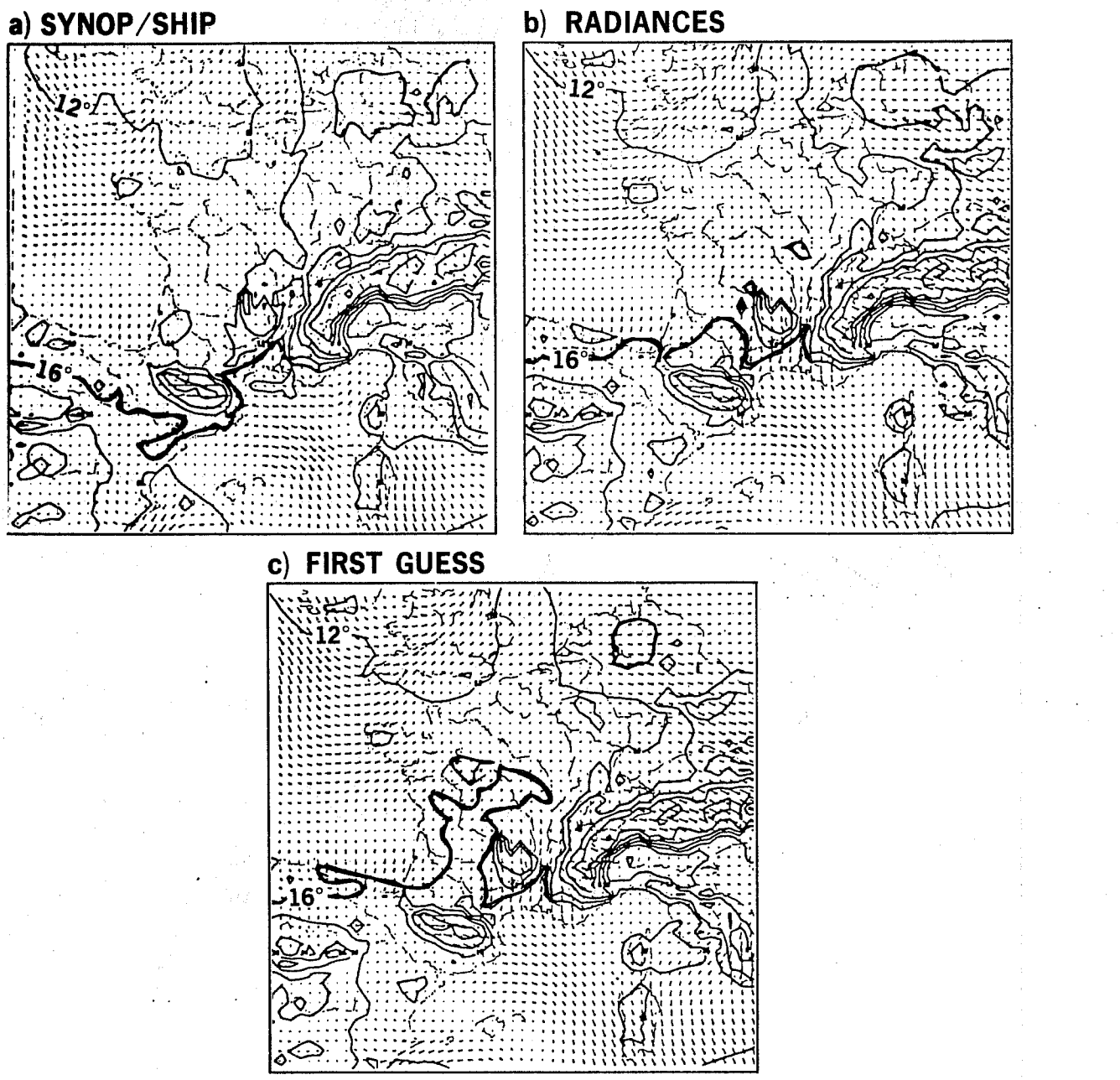

Fig. 10 Temperature and wind analyses at σ = 0.998 for 00 GMT 18/6/85 using (a) only SYNOP/SHIP observations and (b) only radiances; (c) is the first guess taken from the hemispheric analysis.

DATE	F/C	RH 700 hPa	PRECIPITATION	NEBULOSITY LOW	NEBULOSITY MEDIUM	COMMENTS
21/4 6h	6	+ / - -	0	0	+ + / -	- Belgian nebulosity
21/4 12h	12	+ + / - -	+	+ / -	+ + / - -	+ England and Pyranies
22/4 6h	6	+	+	0	+	+ Perturbation middle France
22/4 12h	12	+	+	+	+	+ Undulation near Bordeaux
23/4 6h	6	+ +	+	+	+	+ Front Pyranies - Sardinia
23/4 12h	12	+ / -	+	+	+	+ Alps and Italy
24/4 6h	6	+	+	+	+	+ Eastern Front
24/4 12h	12	+	0	+	+	+ Southern France

+ : impact > 0 of radiances at one place
- : impact < 0 of radiances at one place
+ + : impact > 0 of radiances at many places

Fig. 11 Summary of the impact of radiances on forecasts (without assimilation).

initialization. At that time forecasts from analyses "WITH" or "WITHOUT" gave exactly the same results if normal mode initialization was used. Normal mode initialization seemed to reduce the radiance correction. But it should be noted that in this earlier version of the analysis there was no correction of the wind field due to the radiances ($r(\xi R^{\vartheta}, \xi Z^{\vartheta}) \simeq 0$) and it seems that the imbalance between the mass and velocity fields was corrected by the initialization which seems to retain the wind at this scale. Moreover a new version of nonlinear normal mode initialization has been developed and Craplet (1985) has shown that it does not alter the positive impact observed in some forecasts in June 1984. This version is now regularly used together with the mesoscale analysis.

As in our previous experiments (cf. preceding references) the impact only appears in "physical" fields: nebulosity, precipitation, humidity. In spite of the energetic action of boundary conditions which makes that the model quickly forget its initial conditions to the profit of lateral conditions, it seems that when physical processes are well initialized the forecast of the humidity related fields differ, whereas the forecast of the geopotential, wind and temperature are very similar.

Forecast based on situations in mid-April 85 did not show representative differences (high pressures over the area) though the lack of cloud means that many radiances were used in the analysis. The meteorological situation changed near the 21st and so differences become apparent in the two forecasts.

a) 21st April, 6 GMT : (Fig. 12) The impact is very doubtful. In the humidity we have an underestimation at 700 hPa over England in "WITHOUT", though it appears better in the western part of France. A Mediterranean perturbation is not well seen. The medium level nebulosity reflects the same problem. We have clouds over England only in "WITH" which does not produce enough nebulosity over the western part of France; there are only clouds over the Pyrenees in "WITH".

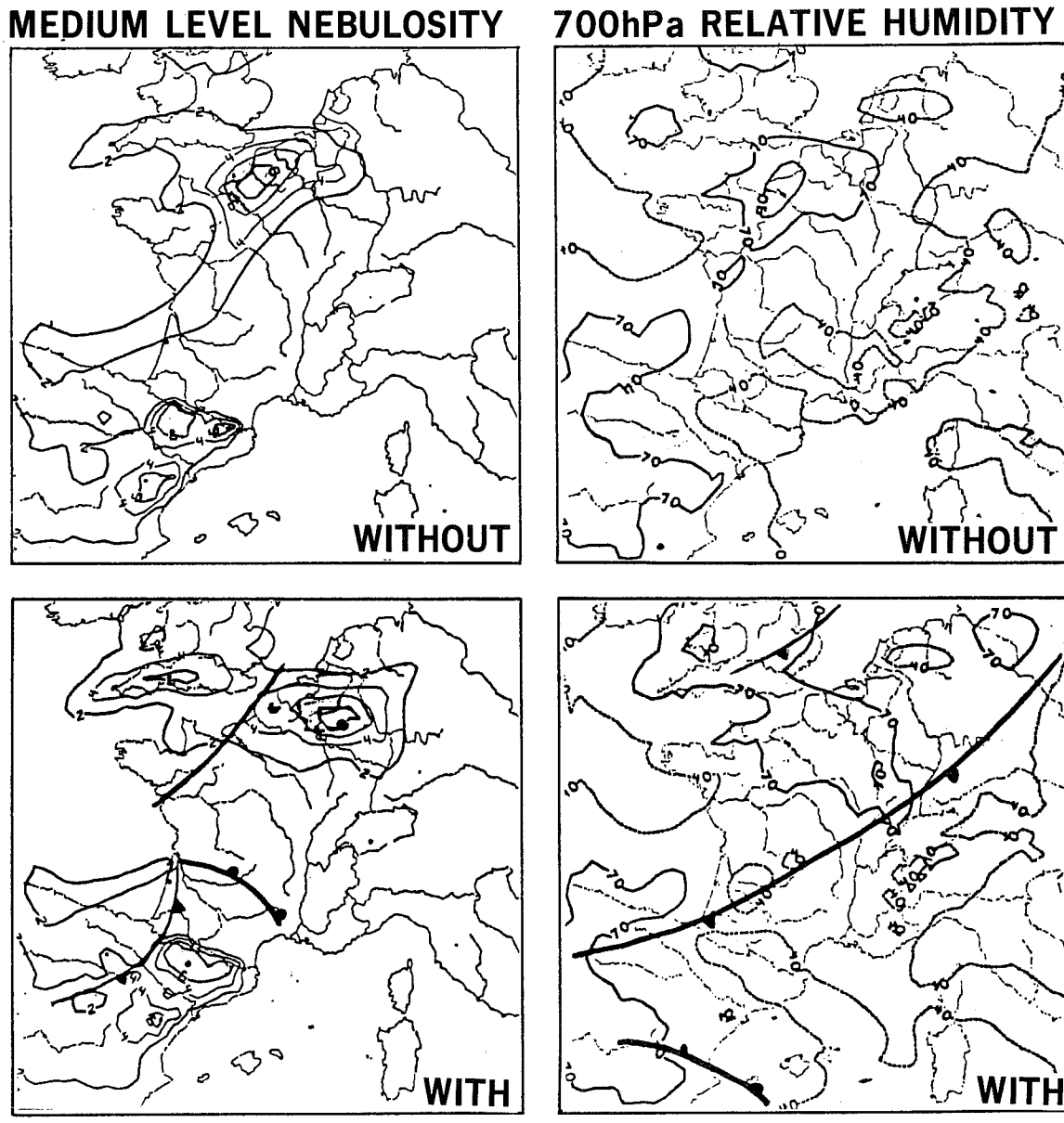

Fig. 12 12 h forecasts of medium level nebulosity valid 12 GMT 21/4/85 and 6 h forecast of 700 hPa relative humidity valid at 06 GMT 21/4/85.

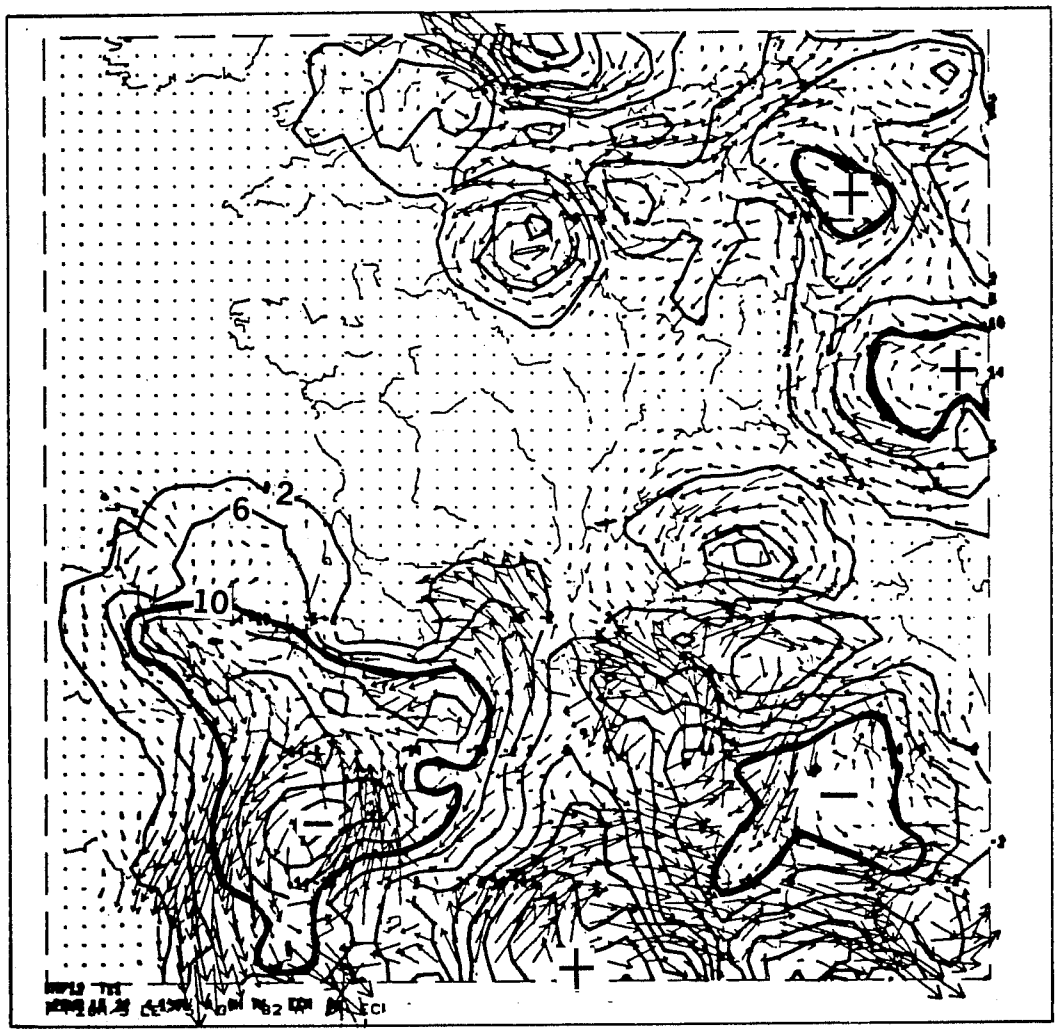

Fig. 13a Differences between WITH and WITHOUT analyses of wind and temperature at 500 hPa at 00 GMT 22/4/84.

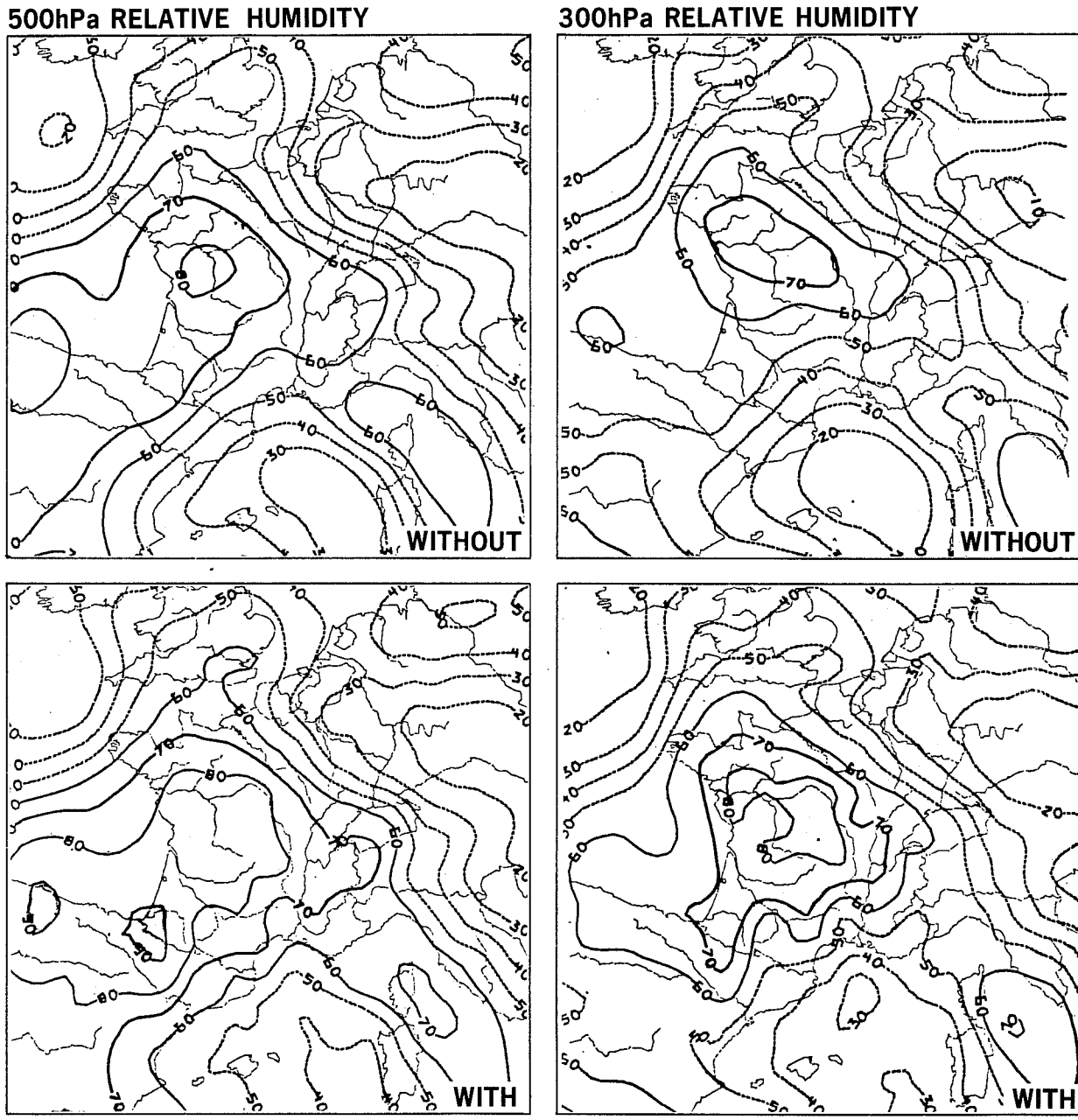

Fig. 13b Analysed relative humidity at 00 GMT 22/4/85 at 500 and 300 hPa.

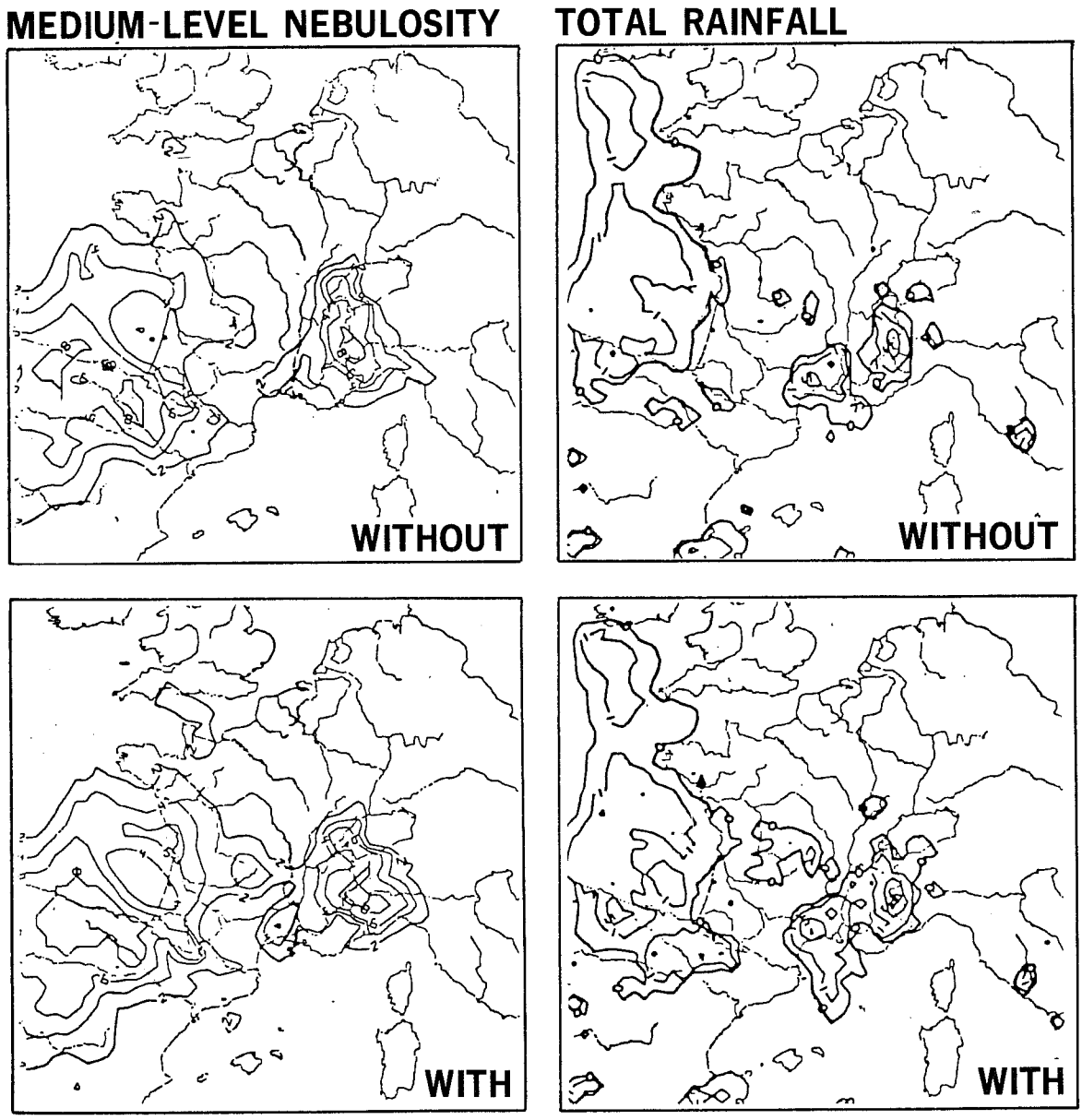

Fig. 13c 6 h forecast of medium level nebulosity and total rainfall valid 06 GMT 22/4/85.

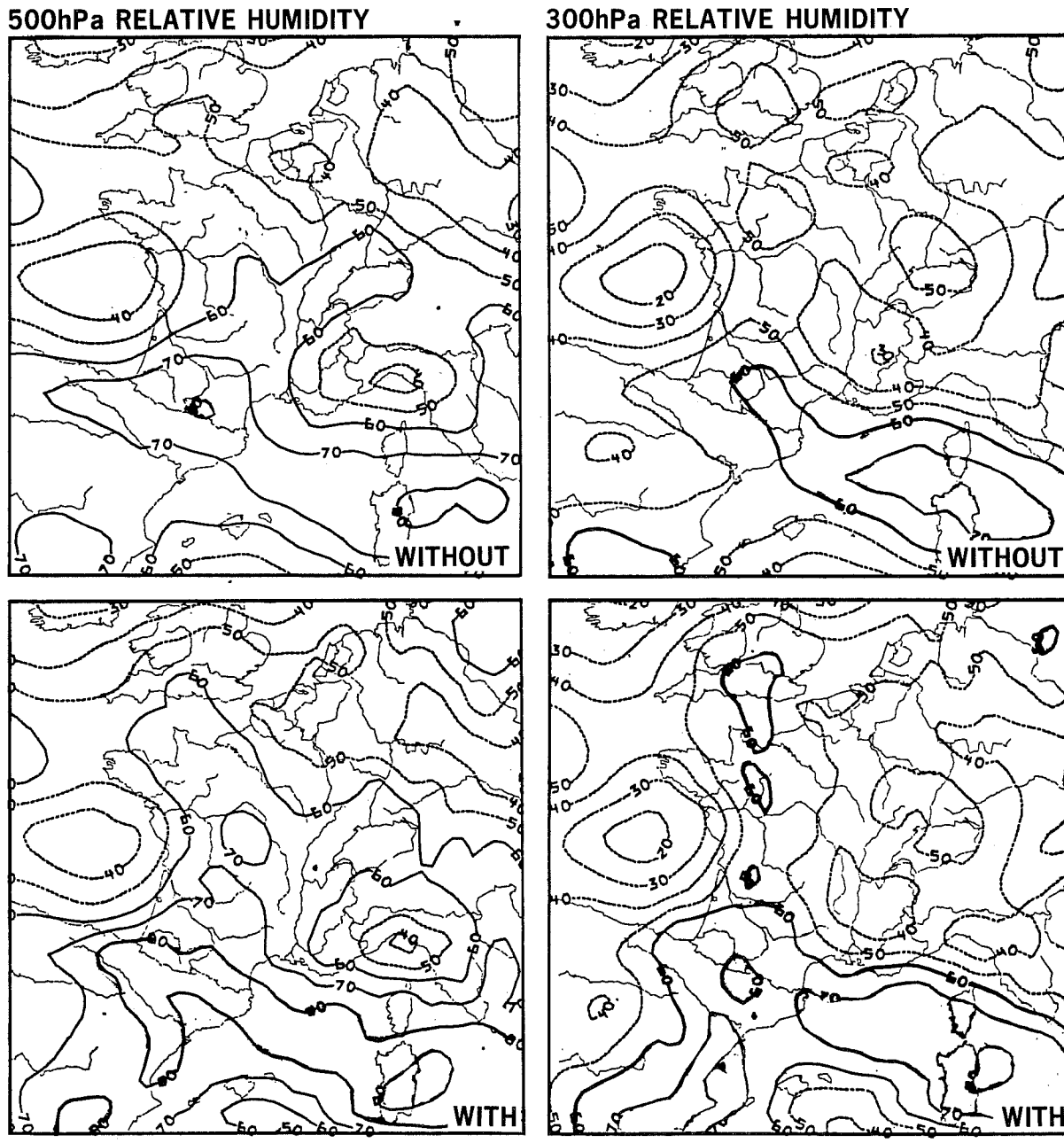

Fig. 14a Analysed relative humidity at 500 and 300 hPa at 00 GMT 23/4/85.

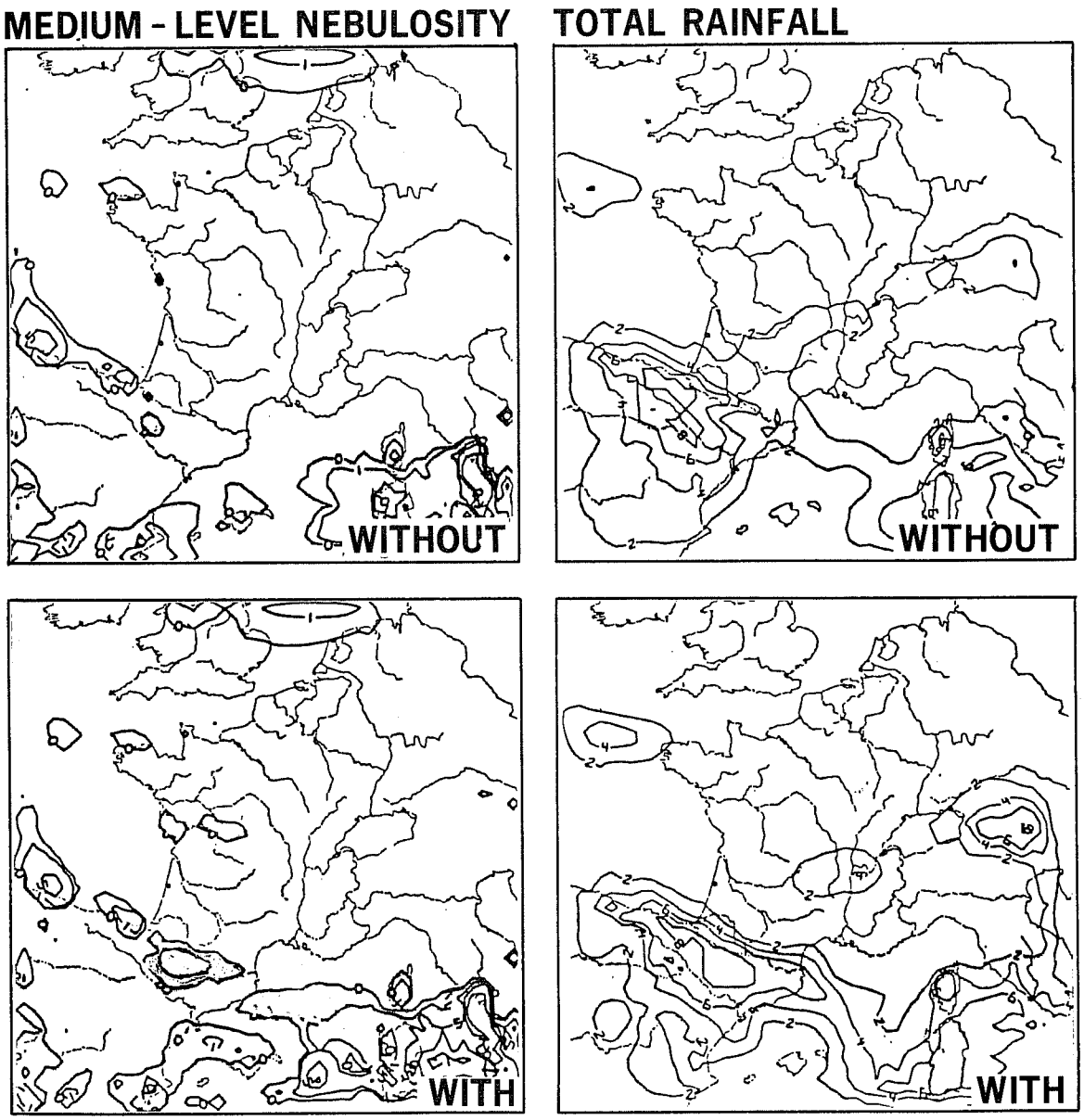

Fig. 14b 12 h forecast of medium level nebulosity and total rainfall valid 12 GMT 23/4/85.

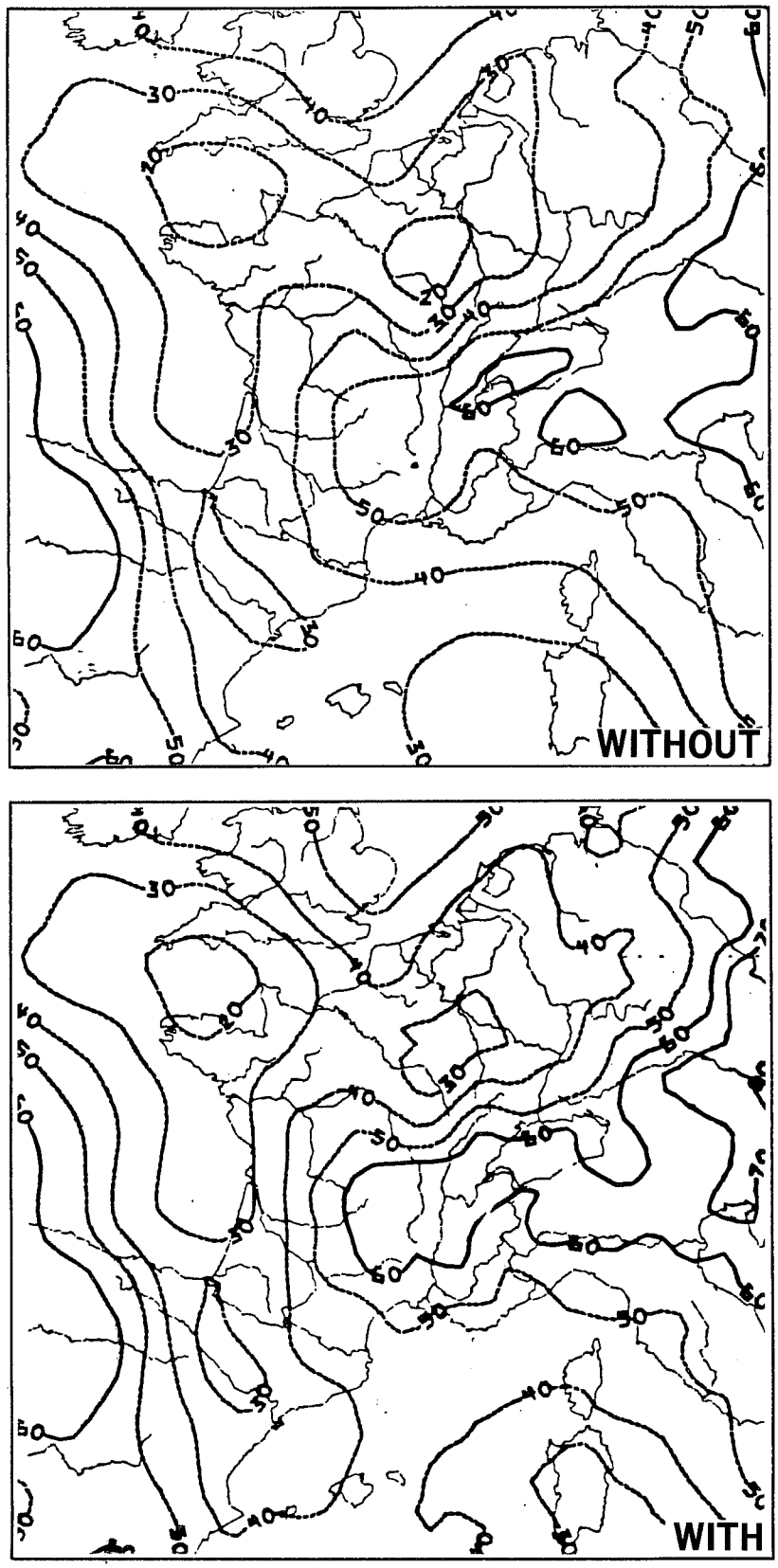

Fig. 15a Analysed relative humidity at 500 hPa at 00 GMT 24/4/85.

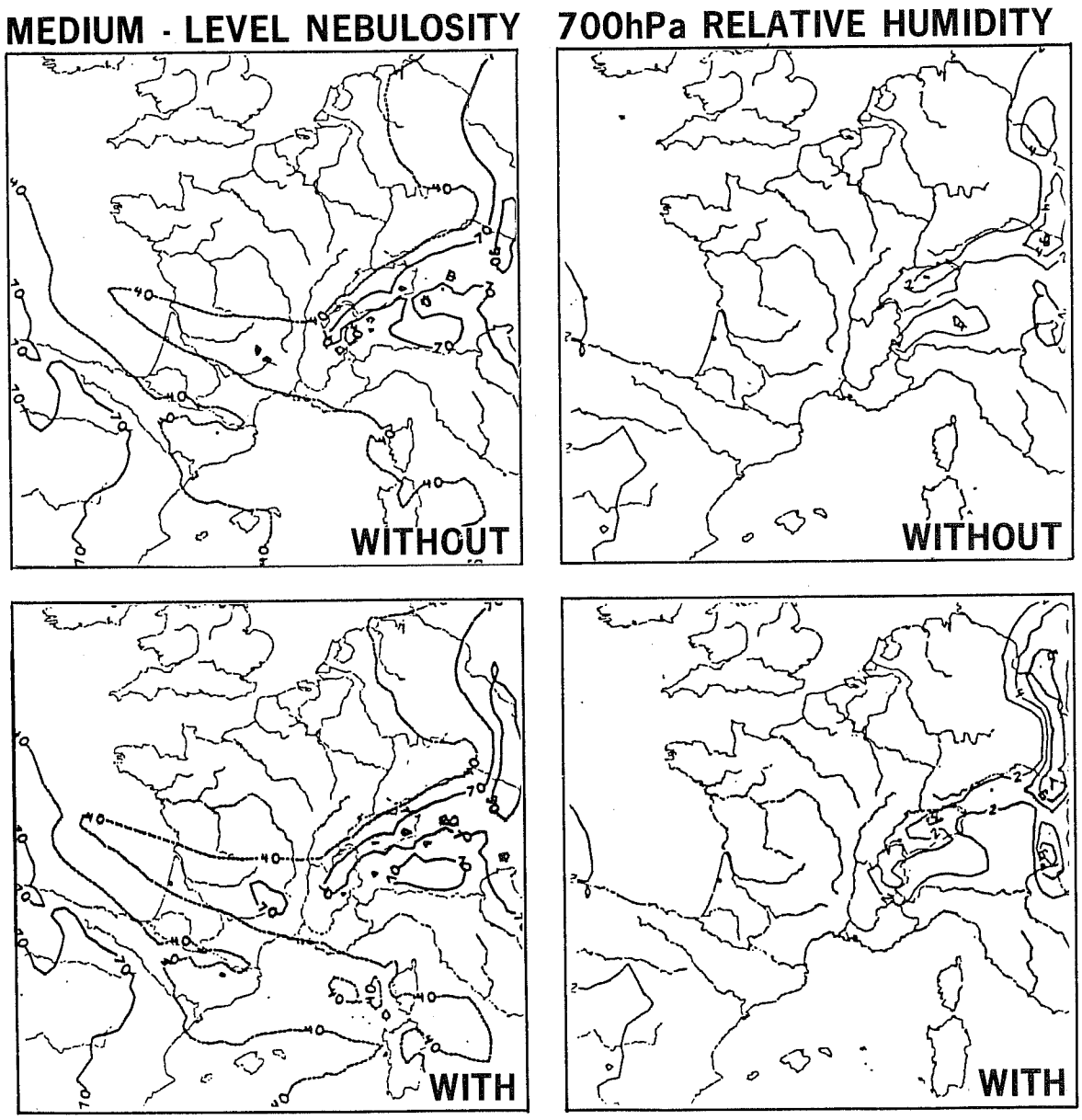

Fig. 15b 12 h forecast of medium level nebulosity and 700 hPa relative humidity valid 12 GMT 24/4/85.

21st April, 12 GMT : the uncertainty remains. The "WITH" experiment creates quite unreasonably a centre of nebulosity and humidity (not precipitation) over the eastern part of Belgium. Nevertheless the precipitation is better treated (important rain in reality) as are the nebulosity and the humidity. In "WITH" there is also a little more nebulosity over the Pyrenees, but the two runs do not reproduce the nebulosity over southwest France.

This situation illustrates also the actual imperfections of the forecast model and the difficulties of using it as a reference.

b) 22nd April 0 GMT (Fig. 13a, b, c) : the analysis "WITHOUT" seems a little dry.

22nd April 6 GMT : Rainfall and nebulosity are much better in "WITH" with regard to the perturbation centred near Bordeaux.

22nd April 12 GMT : Same remark as at 6 GMT ; a perturbation over the north of France is ignored by the two experiments.

c) 23rd April 0 GMT (Fig. 14a, b) : the analysis "WITH" is more moist near Corsica and Italy where rain is observed. It also suggests a better cold front near the eastern cost of Spain.

23rd April 6 GMT : Perturbation over north Spain and Sardinia are better in "WITH" (corresponding to the manual analysis).

23rd April 12 GMT : Same as above but in both cases the precipitation seems overestimated near Italy.

d) 24th April 0 GMT (Fig. 15a, b) : the eastern perturbation is better reproduced in the "WITH" analysis.

24th April 6 GMT and 12 GMT : Same as in the analysis ; the "WITH" forecast describes better the eastern perturbation and its extension over the southern part of France.

7. CONCLUSION AND FUTURE PERSPECTIVES

The preliminary conclusion from these April 85 runs is that we get identical forecasts with fine weather (before 21st) in spite of the different "WITH" and "WITHOUT" analyses. The 21st case is very doubtful, with positive and negative aspects for the two analyses. The 22nd and 23rd situations show a well marked positive impact for the "WITH" analyses, while the impact is a little weaker on the 24th.

We have decided to continue to try to insert radiances in our mesoscale analysis and to evaluate their impact. In order to perform better experiments which could also be used operationally we think it is necessary to have a intermittent mesoscale assimilation ; we are going to test it in a few months. The major advantage will be a better use of asynoptic observations (21 GMT). We shall also be able to use fully the mesoscale forecast model which will allow us to obtain better guess structures, especially in low levels.

The first problem is the spin-up time of the model which has to be reduced. The second one is the macroscale forcing over the mesoscale assimilation system. For this we expect to keep the macroscale part of the hemispheric analysis and to add to it the mesoscale details obtained from the mesoscale analysis. This separation between scales can be performed by using a two-dimensional Fourier decomposition of the field minus another one having the same boundary conditions (obtained by $\nabla^2 x = 0$, for instance) which gives a field with zero over the boundaries. The Fourier decomposition is then separated into macro and meso parts. The same decomposition is done over the two analyses.

Acknowledgements :

I am happy to acknowledge people from Centre de Météorologie Spatiale (Lannion, France) who have made possible these experiments, especially Marcel Derrien and Thierry Phulpin who prepared the satellite data to be inserted in the analysis.

I thank very much Bob Riddaway for his useful advice concerning this paper, and Patricia Audouard for expertly typing the manuscript.

The research reported here has been supported by the Institut National des Sciences de l'Univers (ATP - Recherches Atmosphériques - Contrat 1985 n° 5622) and the computer time has been attributed by the Conseil Scientifique du Centre de Calcul Vectoriel pour la Recherche.

REFERENCES

Bergman, K.H., 1979 : Multivariate analysis of temperatures and winds using optimum interpolation. Mon. Wea. Rev., 107, 1423-1444.

Brière, S., 1982 : Nonlinear Normal Mode Initialization of a Limited-Area Model, Mon. Wea. Rev., 110, 1166-1186.

Craplet, A., 1985 : Initialisation par modes normaux du modèle Péridot. Note Technique de l'EERM in preparation. Available EERM/CRMD, 2 Avenue Rapp - 75007 PARIS.

Durand, Y., 1983 : Développement d'un système d'analyse fine sur domaine limité. Internal report. Available EERM/CRMD, 2 Avenue Rapp - 75007 PARIS.

Durand, Y., Juvanon du Vachat R., 1983 : Mesoscale Analysis using satellite information. Technical Proceedings of the First International TOVS Study Conference (Igls, September 1983). p. 80-93.

Durand, Y., Juvanon du Vachat R., 1985 : Developments of a mesoscale analysis using raw satellite data. Technical Proceedings of the Second International TOVS Study Conference (Igls, February 1985) to appear.

Pailleux, J., 1984 : Testing the North Atlantic observing network using different analysis schemes. ECMWF Seminar on Data Assimilation and Observing Systems (September 1984). p. 321-324.

Pham, H.L., Rousseau, D. and Juvanon du Vachat, R., 1983 : Simulations à échelle fine dans le cadre du projet Péridot. Note technique de l'EERM n° 59. Available EERM/CRMD, 2 Avenue Rapp -75007 PARIS.

Smith, W.L., 1979 : Determination of vertical temperature profiles. UN/WMO Training Seminar.